X-640-72-417

PREPRINT

NASA TM X-66101

COOLING OF DENSE STARS

SACHIKO TSURUTA

OCTOBER 1972

GODDARD SPACE FLIGHT CENTER
GREENBELT, MARYLAND

X-640-72-417
Preprint

COOLING OF DENSE STARS*

Sachiko Tsuruta**

October 1972

*Paper presented at IAU Symposium No. 53, "Physics of Dense Matter," University of Colorado, Boulder, Colorado, August 21-26, 1972.

**National Academy of Science-NRC Senior Research Associate at NASA, Goddard Space Flight Center.

Goddard Space Flight Center
Greenbelt, Maryland

CONTENTS

COOLING OF DENSE STARS

Sachiko Tsuruta

ABSTRACT

Cooling rates are first calculated for neutron stars of about one solar mass and 10 km radius, with magnetic fields from zero to about 10^{14} gauss, for two extreme cases of maximum and no superfluidity. The results show that most pulsars are so cold that thermal ionization of surface atoms would be negligible.

Next, nucleon superfluidity and crystallization of heavy nuclei are treated more quantitatively, and more realistic hadron star models are chosen. Cooling rates are thus calculated for a stable hyperon star near the maximum mass limit, a medium weight neutron star, and a light neutron star with neutron-rich heavy nuclei near the minimum mass limit. Results show that cooling rates are a sensitive function of density. The lightest star is cooler than others in earlier stages but the trend is reversed later. The medium weight star is generally the coldest of all in lower temperature regions where the effect of superfluidity becomes significant. However, if a heavy star contains pions, its cooling will be even faster.

The Crab pulsar and Vela pulsar, expected to be the youngest two, can be as hot as $(2 \sim 4) \times 10^6$ °K (on the surface), comparable with the results obtained from internal frictional heating by Greenstein, if they are medium weight to heavy hadron stars. However, older pulsars are cold. In fact, at about a few million years, the age of average radio pulsars, the surface temperature becomes only several hundred to several thousand degrees. Thus, the earlier conclusions about cold pulsars are still valid.

At the end cooling of a massive white dwarf star is shown.

COOLING OF DENSE STARS

I. INTRODUCTION

In recent years considerable progress has been made in the studies of cold dense matter (the earlier reports in this symposium by Professor Bethe (1972a) and others). In the present talk, we wish to report some recent work on thermal properties of dense stars.

Some years ago when the first few of the galactic X-ray sources were discovered, it was suggested that these X-ray sources might be neutron stars. The detailed account was reviewed, for instance, in the paper by Tsuruta and Cameron (1966a). The conclusion was that the cooling rate alone could not exclude the possibility of detecting neutron stars as X-ray emitters, but that the observed spectra of X-rays from these sources were inconsistent with those of blackbody radiation expected from the surface of neutron stars. This and other considerations led us to doubt the prospect of ever observing neutron stars. The discovery of pulsars several years ago, however, changed the whole picture. Now it is generally believed that pulsars are rotating, magnetic neutron stars (Gold 1968). Moreover, theoretical considerations and some observational evidence (such as the speed-ups of the Crab and Vela pulsars) suggest the presence of superfluid in neutron stars (Ginzburg 1971, Pines 1972, Borner and Cohen 1972, etc.). In the earlier cooling calculations the effect of magnetic fields and superfluidity was not taken into account. In our recent work, therefore, emphasis was placed on the effect of these new factors, which was expected to reduce cooling rates significantly. The new outcome may prove valuable for the understanding of pulsar and X-ray star problems.

In the next section, II, basic equations are introduced. In section III (a) we summarize the general effect of strong magnetic fields and superfluidity on neutron star cooling, a joint work of Ruderman, Canuto, Lodenquai and myself, published in Tsuruta, et. al. 1972. In recent months I tried to treat the problem more quantitatively using realistic hadron star models and other newly available information. (The name "hadron star" is used when we collectively call all dense stars with central density greater than about 10^{14} gm/cm^3, for they are generally composed of a variety of hadrons.) The results are reported in section III (b). Cooling of white dwarfs is discussed in the last section, III (c).

II. BASIC EQUATIONS

Cooling time t is obtained by

$$t = \int_{U_0}^{U_t} \frac{dU}{\bar{L}(U)}, \tag{1}$$

where U_0 and U_t are energy of the star at t = 0 and at time t, respectively, and $\bar{L}(U)$ is the average luminosity while the energy changes by dU. The total energy is mainly a function of the internal temperature of the star T_i and expressed as

$$U = U(T_i) = \sum_k U_k^D + U_{ion}^N \text{ (with k = n, p, e, m, h)}, \tag{2}$$

the sum of the thermal tail of degenerate particles k and energy of non-degenerate heavy ions. The possible degenerate particles k in hadron star matter include neutrons (n), protons (p), electrons (e), mesons (m), and hyperons (h).

The total energy loss rate L is

$$\begin{aligned} L &= L_\gamma + L_\nu, \\ L_\gamma &= L_\gamma(T_e) = 4\pi\sigma R^2 T_e^4, \\ L_\nu &= L_\nu(T_i) = L_\nu^u + L_\nu^B + L_\nu^{pl} + L_\nu \text{ (others)}. \end{aligned} \tag{3}$$

L_γ is photon luminosity and L_ν is neutrino luminosity. The superscripts u, B, and pl stand for the URCA neutrino process, the neutrino bremsstrahlung process, and the plasmon process, respectively. T_e is the surface temperature of the star, R is the stellar radius and σ is Stefan's constant. L_ν (others) includes photo-neutrino process, pair annihilation process and neutrino synchrotron process. In the earlier stages of cooling when temperatures are high neutrino emission dominates, while later at lower temperatures photon emission is more significant. In the absence of magnetic fields and superfluidity, the URCA process is dominant among neutrino processes, the plasmon process competes with it at higher temperatures and bremsstrahlung at lower temperatures. At extremely high temperatures ($T > 10^{10}$ °K) pair annihilation becomes significant, but contribution by other processes are relatively minor.

Total energy and neutrino luminosity depend on internal temperature, while photon luminosity is a function of surface temperature. Thus, the first step is to find relation between T_i and T_e. For this purpose the energy transfer equation and hydrostatic equations are integrated over the outer layers from the surface to the point where temperature gradient disappears. Recent studies suggest that a neutron star has a distinct boundary with $\rho_s \simeq 10^4$ gm/cm^3 with a sharp, discontinuous density drop (Ruderman 1972). Therefore, this integration was performed both from the photosphere and from the boundary with $\rho_s = 10^4$ gm/cm^3. For magnetic neutron stars with $H \gtrsim 10^{12}$ gauss, both led to similar results. Convection is very unlikely in neutron stars (Tsuruta 1964), so that energy transfer will be governed by radiation. The basic equations are therefore expressed as

$$\frac{dT}{dr} = \frac{-1}{4\pi r^2} \frac{3}{4ac} \frac{K\rho}{T^3} L$$

$$\frac{dP}{dr} = - \frac{G(P/c^2 + \rho)\ (4\pi r^3\ P/c^2 + m)}{r(r - 2m\ G/c^2)}\ ,$$

$$\frac{dm}{dr} = 4\pi\rho\, r^2, \tag{4}$$

with the equation of state

$$P = P(\rho,\ T),$$

which becomes degenerate at higher densities ($\rho \gtrsim 10^4$ to 10^6 gm/cm^3 depending on temperatures). In the above equations standard notation is used (see, for instance, Schwartzschild 1958). General relativistic form is used for hydrostatic equations because this effect is not negligible near the surface of a neutron star (Tsuruta and Cameron 1966a).

The opacity which appears in the transfer equation is expressed as

$$\frac{1}{K} = \frac{1}{K_R} + \frac{1}{K_c}, \tag{5}$$

where K_R and K_c are the radiative and conductive opacity, respectively. Radiative opacity is due to various photoelectric processes (free-free, bound-free, and bound-bound transitions) and scattering by electrons (Compton scattering at $T > 5 \times 10^8$ °K and Thomson scattering at lower temperatures).

III. RESULTS AND CONCLUSIONS

(a) General Effects of Magnetic Fields and Superfluidity on Cooling

For this purpose we chose a medium mass neutron star model V_γ (II), with the V_γ type potential of Levinger and Simmons and the composite equations of state with equilibrium compositions, constructed by Tsuruta and Cameron (1966b). (See also Hartle and Thorne 1968.) It has the following properties; stellar mass $M = 1.07M_\odot$, radius $R = 12.33$ km, and central density $\rho^c = 7.39 \times 10^{14}$ gm/cm^3.

The major effect of strong magnetic fields is to drastically reduce photon opacity in certain directions. It also reduces significantly the URCA neutrino luminosity. The effect of the presence of superfluidity is mainly to reduce total energy of superfluid particles at lower temperatures. It also supresses the URCA luminosity.

First, consider the effect of magnetic fields on opacity. We have found that the following approximation is valid for the radiative opacity in superstrong magnetic fields with $H \gtrsim 10^{12}$ gauss (see Tsuruta, et. al. 1972; Lodenquai, et. al. 1972; Canuto, Lodenquai and Ruderman 1971; Canuto 1970):

$$\sigma_\omega(H) = \left(\frac{\omega}{\omega_H}\right)^2 \sigma_\omega(0), \quad \text{for} \quad \omega << \omega_H, \tag{6}$$

where ω is the radiation frequency, $\omega_H = eH/m_e c$ is the electron cyclotron frequency, and σ_ω (H) and σ_ω (0) are the photon cross section with and without a magnetic field, respectively. The Rosseland mean was used to take account of the frequency dependence. The radiative opacity, thus obtained, can be expressed as

$$K_R(H) = a_R K_R(0); \quad \text{with} \quad a_R \propto \left(\frac{T}{H}\right)^2, \quad \leq 1 . \tag{7}$$

The conductive opacity is similarly expressed as

$$K_c(H) = a_c K_c(0); \quad a_c \leq 1. \tag{8}$$

The correction factor a_c is generally a complicated function of a magnetic field, density and temperature. In the inner degenerate layers where the conductive opacity plays the dominant role, the temperature dependence drops out and the factor a_c decreases with increasing magnetic fields and decreasing density. In Figure 1, the density dependence of the factor a_c is shown for different magnetic field values in the regions of our interest. Here, $\theta = H/H_q$, with $H_q = m_e^2 c^3/\hbar e = 4.41 \times 10^{13}$ gauss. (Similar calculations were made by Canuto and Chiu (1969)

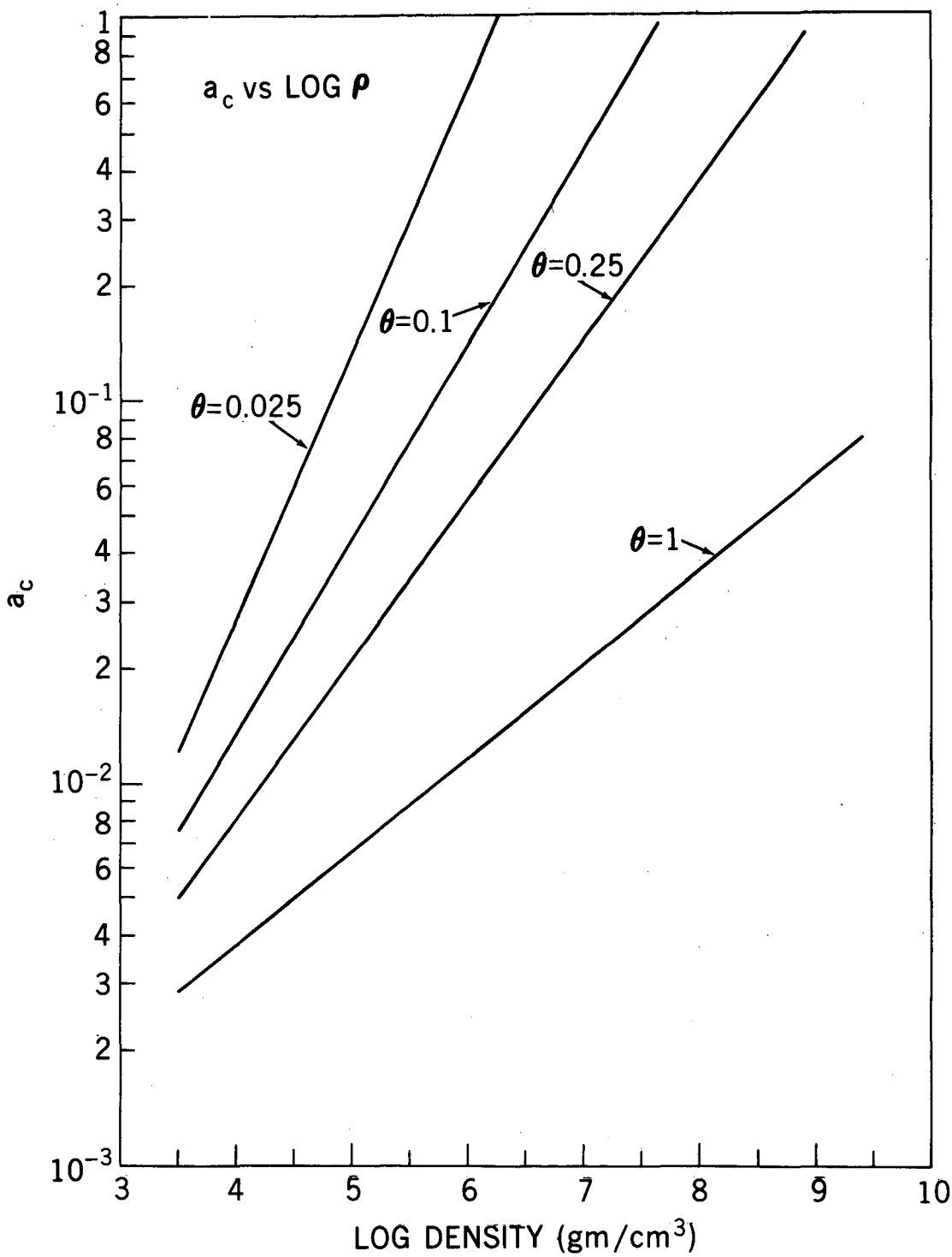

Figure 1. The factor a_c as a function of density. The a_c is the ratio of conductive opacity with magnetic fields to that without magnetic fields, $K_c(H)/K_c(0)$. $\theta = H/H_q$, and $H_q = 4.41 \times 10^{13}$ gauss.

for $\theta = 1$ and 0.1 in the vicinity of $\rho \simeq 10^6$ gm/cm^3.) We have applied these correction factors to the zero field opacities previously obtained by Tsuruta and Cameron (1966a). It may be noted that electrons become relativistic for densities $\rho \gtrsim 10^6$ gm/cm^3. In these high density regions, therefore, we used the general formula for conductive opacity (which applies to both relativistic and non-relativistic cases), given in WHITE DWARFS by Schatzman (1958). (In the earlier work where Cox's opacity code was used for zero field opacities, the relativity effect was not included. I owe Professor Hayashi (1971) for pointing out this to me.)

In Figure 2, the relation between T_i and T_e thus obtained is shown for varying strengths of magnetic fields. In the curve (I), H = 0. The curve (II) corresponds to a star of constant field strength of about 10^{12} gauss. In the curve (III), the surface field is the same as in (II) but the internal field is increased by a factor of 10. We note that the difference between the internal temperature and surface temperature decreases with increasing H and decreasing T. When $H \gtrsim 10^{12}$ gauss, this difference almost vanishes for $T \lesssim 1000$ °K.

In order to study the effect of superfluidity, the following two extreme cases are studied. In Case (S) (= maximum superfluidity), the energy of superfluid particles (neutrons and protons) is set equal to zero, and thus degenerate electrons are the main contributors to the total energy. In Case (N) (= normal state), superfluidity is completely neglected, and thus degenerate neutrons are the main contributors to the total energy. These effects on the URCA luminosity are also maximized. Thus, we set $L_\nu^u = 0$ for all models in Case (S) and for $H \geq 10^{12}$ gauss in Case (N). The results are shown in Figures 3 and 4, where internal temperatures and surface temperatures, respectively, are plotted as a function of time for different magnetic field strengths. The solid curves stand for Case (S) (= exaggerated superfluidity) and the dashed curves represent Case (N) (= no superfluidity).

We note that the effect of both strong magnetic fields and superfluidity are important for neutron stars older than about 100 years. For instance, at t = 1000 years which corresponds to the approximate age of the Crab pulsar NP 0532, the surface temperature is anywhere between $\sim 10^5$ °K and a few times 10^7 °K. For the Vela pulsar (with $t \simeq 10^4$ years) it is between 10^4 °K and 10^7 °K. However, for typical older pulsars of a few million years (so far observed only as radio pulsars), the star seems very cold (with the surface temperature anywhere between about several hundred degrees and about 10^3 times higher).

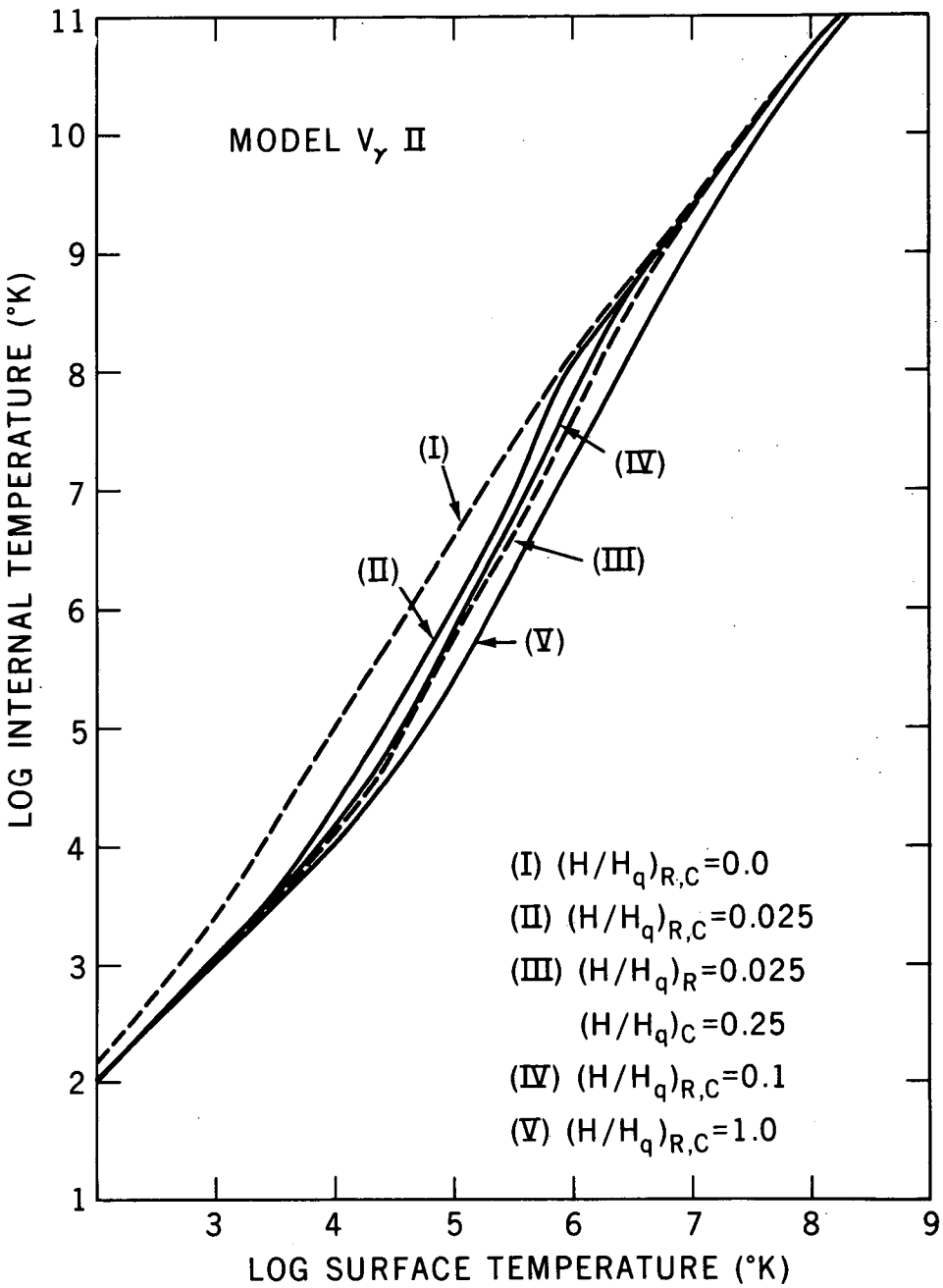

Figure 2. Internal Temperature as a function of surface temperature at different magnetic field strengths, for Model V_γ II as described in section III(a). Curves (I), (II), (IV) and (V) stand for a uniform magnetic field of strengths (H/H_q) =0, 0.025, 0.1 and 1, respectively. In the curve (III), the surface field strength is the same as in the curve (II), but the internal field strength is increased by a factor of 10.

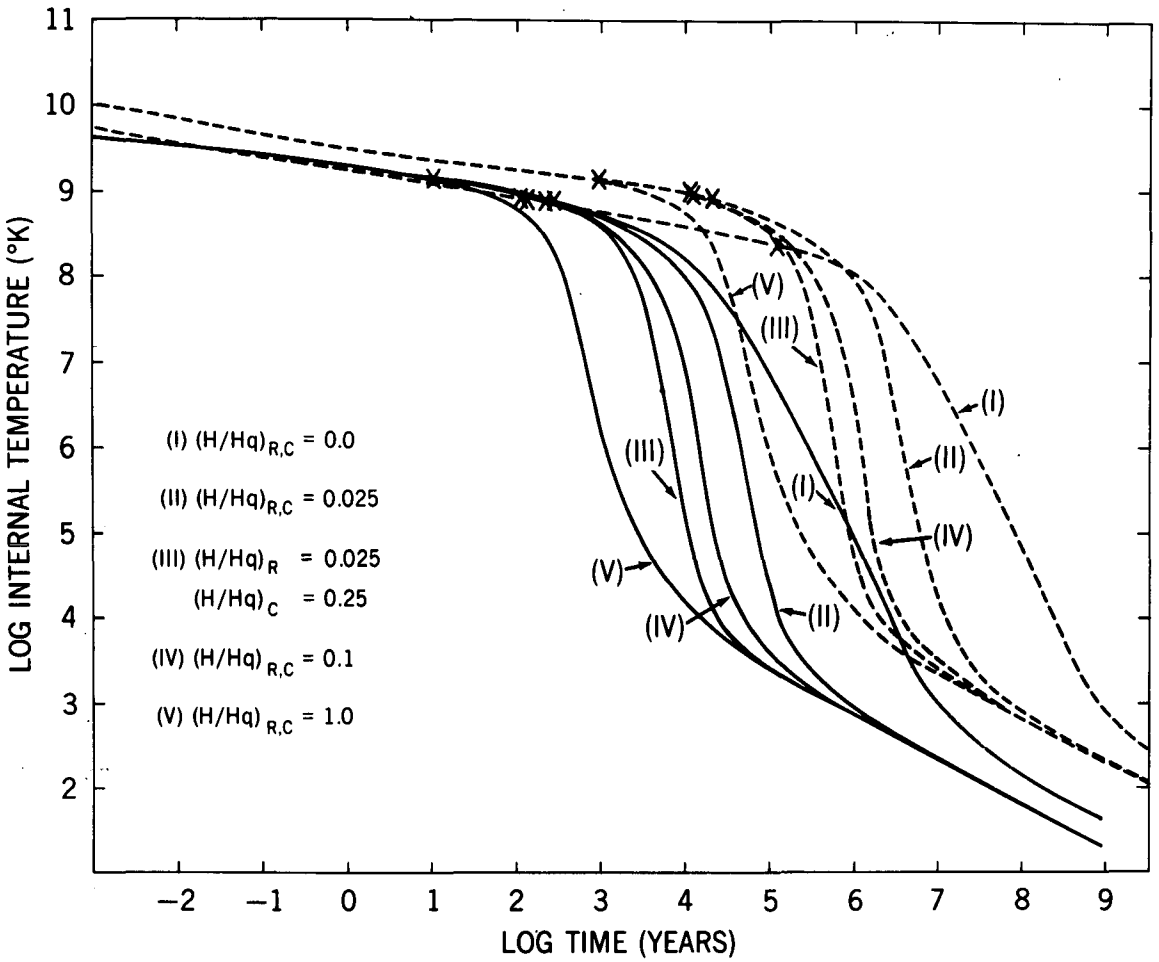

Figure 3. Internal temperature as a function of time for Model V_γII at different magnetic field strengths. Notation is the same as in Figure 2. The points where the major cooling mechanism shifts from the neutrino emission to the photon emission are indicated by the crosses. The solid curves and dashed curves represent two extreme cases of maximum and no superfluidity, respectively, as explained in the text.

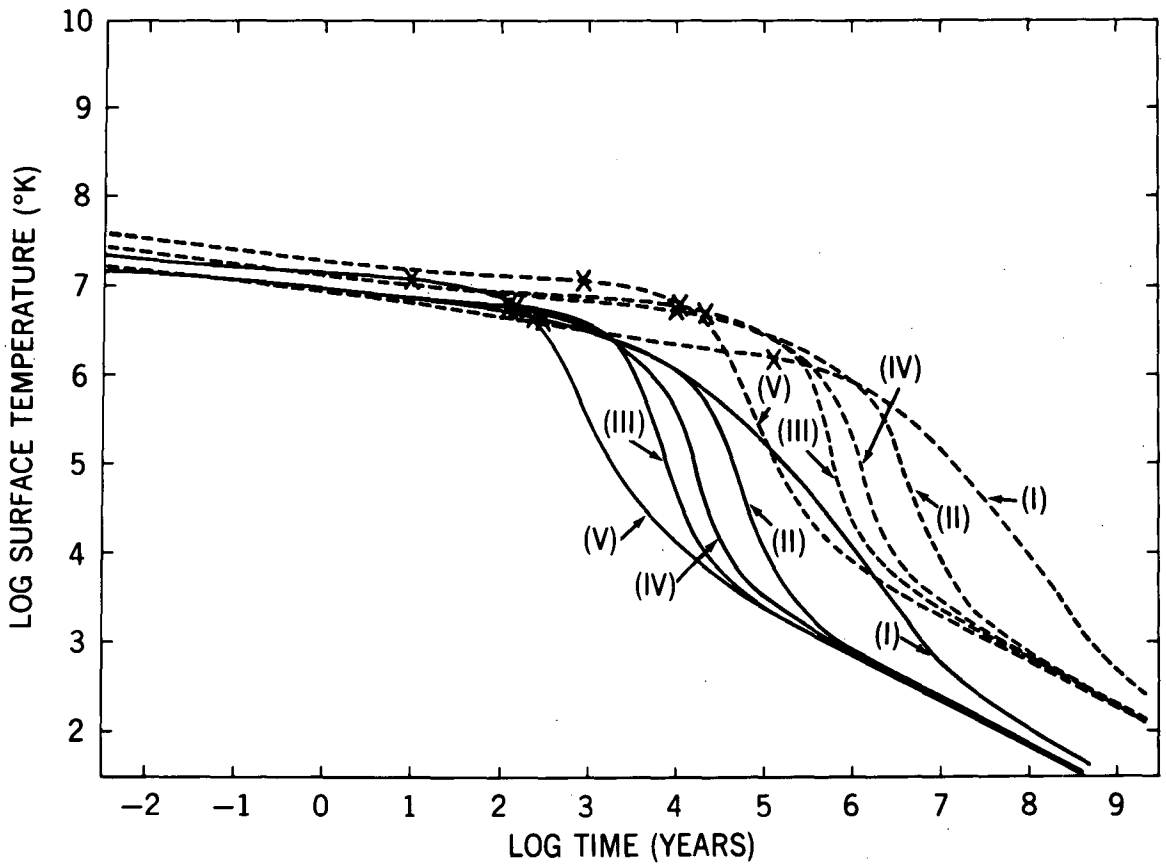

Figure 4. Surface temperature as a function of time (cooling curves) for Model V_γII at different magnetic field strengths. Notation is the same as in Figure 3.

(b) Application to Specific Models

In view of the large discrepancy found in the last section between the two extreme cases (of maximum and no superfluidity), it might be worthwhile to treat more exactly the effect of superfluidity. Fortunately, the large uncertainty concerning the superfluid energy gap was greatly reduced according to the latest report from the Kyoto group (Takatsuka 1972, Tamagaki 1972). There, the $^1S_0$-gap and the $^3P_2$-gap, $\Delta(^1S_0)$ and $\Delta(^3P_2)$, are calculated as a function of density by making use of the realistic values of the effective mass, m* (ρ). Due to the slight decrease of the value m*, the gap $\Delta(^1S_0)$ is somewhat reduced but otherwise its general behavior is similar to previous results. There are, however, significant changes in the behavior of the gap $\Delta(^3P_2)$. Taking into account the attractive effect of the $^3P_2 - ^3F_2$ coupling due to the two-nucleon tensor force, Takatsuka (1972) shows that the gap $\Delta(^3P_2)$ behaves like Figure 5. (If the $^3P_2 - ^3F_2$ coupling is neglected, the $^3P_2$-gap becomes negligibly small for

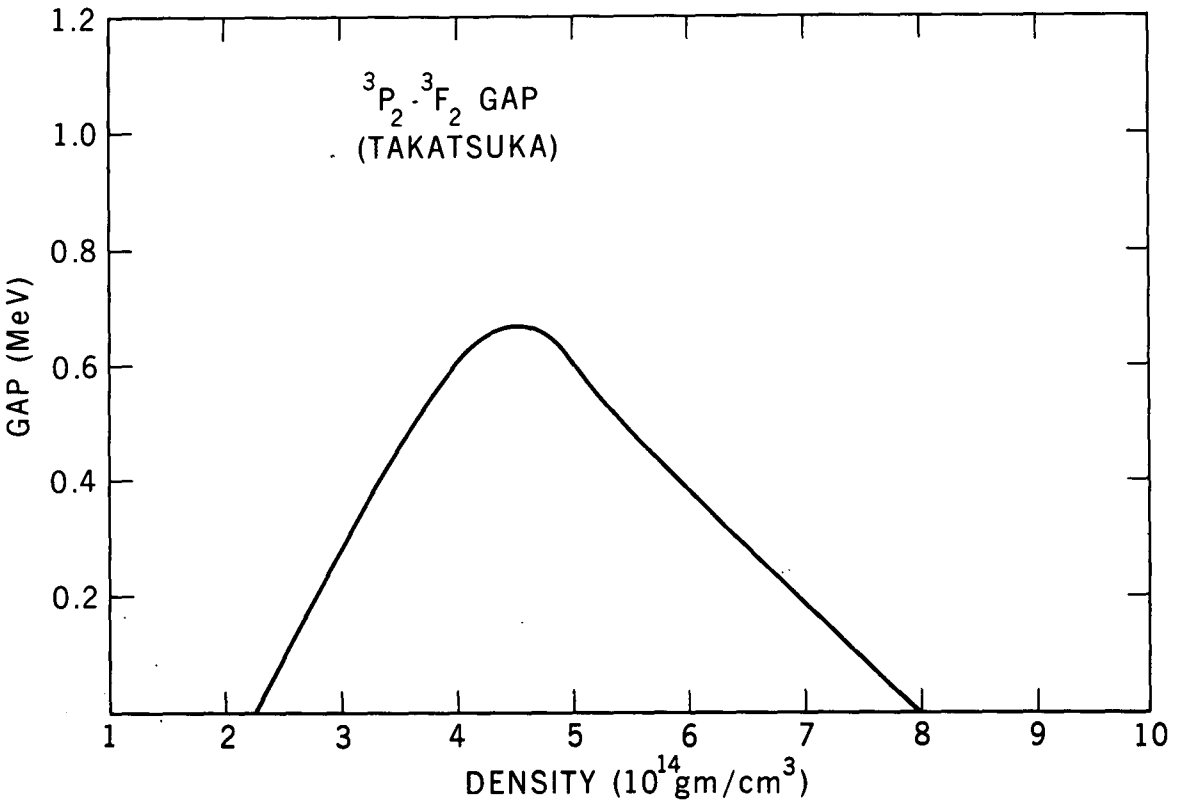

Figure 5. The density dependence of $\Delta(^3P_2)$ calculated by Takatsuka (1972) including the $^3P_2$–$^3F_2$ tensor coupling.

realistic values of m*.) The conclusion is, (i) the $^1S_0$-gap (with maximum $\Delta \simeq 2.5$ Mev) exists in the density region $\rho \simeq (10^{11} \sim 1.5 \times 10^{14})$ gm/cm^3, and (ii) the $^3P_2$ - gap (with maximum $\Delta \simeq 0.65$ Mev) exists in the range $\rho \simeq (2 \sim 8) \times 10^{14}$ gm/cm^3.

It seems clear from the above outcome that the appearance of superfluidity depends critically on the stellar density. If the density goes up as high as $\sim 10^{16}$ gm/cm^3 for stars near the maximum mass limit (as some of neutron star models indicate), the effect of superfluidity will be small. (These heavy stars may possibly contain high concentration of hyperons and may better be called "hyperon stars".) On the other hand, lighter stars near the minimum mass limit may have quite different internal structure; namely, the presence of heavy nuclei in the whole interior (Baym, Pethick and Sutherland 1971). Therefore, three typical models are chosen for the present investigation. These are; Model (I) a heavy hyperon star near the maximum mass limit, Model (II) a medium weight neutron star, and Model (III) a light neutron star near the minimum mass limit whose central core contains heavy nuclei. Their characteristics are summarized in

TABLE I

Characteristics of the three models of hadron stars chosen in section III(b). ρ_c is the central (energy) density in cgs units, $M/M_\odot$ is the mass in solar mass units, and R is the stellar radius in km. Model (I) is a heavy hyperon star, Model (II) is a medium weight neutron star, and Model (III) is a light neutron star with neutron-rich heavy nuclei.

MODEL	CENTRAL DENSITY	MASS	RADIUS	
	ρ^c (gm/cm^3)	$M/M_\odot$	R(km)	
(I)	6.0×10^{15}	1.413	7.10	HEAVY
(II)	8.0×10^{14}	0.476	10.9	MEDIUM
(III)	1.1×10^{14}	0.105	76.7	LIGHT

Table I. In these models the different density ranges are treated in the following manner. (ia) Outermost layers, where density $\rho < \rho_1 \equiv 3 \times 10^{11}$ gm/cm^3: In this region, the temperature dependence of composition cannot be neglected for our present purposes. This is mainly because neutron abundance is significant at higher temperatures, while neutrons disappear in this region at zero temperatures (Salpeter 1961, Wheeler 1966). In fact, it was found that matter becomes predominantly neutrons (with small percentages of α-particles, protons and electrons) for $T \gtrsim 2 \times 10^{10}$ °K. At about four billion degrees where composition freezes, there are still significant number of neutrons present. Also on the high density side ($\rho \gtrsim 10^{11}$ gm/cm^3), heavy nuclei are crystallized before the composition freezes. Therefore, we used the results of recent calculations of equilibrium composition at finite temperatures ($10^9 \sim 5 \times 10^{10}$ °K) by Tsuruta, Truran and Cameron (1972).

(ib) Subnuclear density region, where $\rho_1 \lesssim \rho < \rho_2 \equiv \sim 2 \times 10^{14}$ gm/cm^3: Matter in this region consists of neutron-rich heavy nuclei (A, Z), neutrons and electrons. For the value Z, we used the recent work by Ravenhall, Bennett and Pethick (1972). They show that in this region the value Z is finite and a slowly varying function of density. The ratio A/Z at a given density is more insensitive to different models, and we used the values listed in Baym, Bethe and Pethick 1971. The relative abundance of each component was then calculated using standard method (see the above references).

(ii) Nuclear region, where $\rho_2 \lesssim \rho < \rho_3 \equiv \sim 8 \times 10^{14}$ gm/cm^3: Nuclear physics approach is valid in this region. We assumed the OPEG type potential for nucleon interactions. This is a Gaussian type soft core potential with one pion exchange,

constructed by Tamagaki (1968). The relative abundance of constituents (neutrons, protons and electrons) was found by standard method (see, for instance, Baym, Bethe and Pethick 1971).

(iii) Ultradense region, where $\rho \gtrsim \rho_3$: The presence of hyperons and muons was assumed. Specifically, the hyperonic composition of model (C) by Pandharipande (1971) was adopted. It may be noted that the appearance of hyperons depends critically on the type of strong interactions assumed among baryons. For instance, it was reported (Moszkowski 1972) that at above 6 times nuclear density the most stable configuration is still a neutron gas in a certain case (*1). However, the result of our cooling calculations does not change significantly if our heaviest model is a neutron star instead of a hyperon star.

Using equations (4) to (8), relation between internal temperatures and surface temperatures was obtained for the models (I), (II) and (III) described above. The results are shown in Figure 6. In this connection, we may note the angular dependence of the magnetic reduction of opacity. This problem was taken into account by assuming a dipole field and by the estimate that the reduction as expressed by Equation (6) applies in directions within about 10% along both magnetic poles. This approximation is thought to be sufficient, in view of greater uncertainties involved in the derivation of equations (7) and (8).

In the final cooling calculations, the energy and the URCA rates of superfluid nucleons were treated more accurately. We also included the crystallization of heavy ions. Thus, as the energy of degenerate particles k in Equation (2), we used the following formula:

$$U_k^D = \int C_k^D \, dT, \text{ where}$$

$$C_k^D = \int (c_0)_k^D \, Y_s \, n_k \, 4\pi r^2 \, dr,$$

$$(c_0)_k^D = \left(\frac{\pi^2 k_B^2}{m_k c^2} \, \frac{(x_k^2 + 1)^{1/2}}{x_k^2} \right) T, \qquad (9)$$

$$x_k = P_k^F/(m_k c),$$

$$Y_s = (8.5 \exp(-1.44\, T_c/T)) \frac{T_c}{T}, \quad (T \ll T_c),$$

$$k_B T_c = 0.57 \times \Delta(^3P_2)/\sqrt{2}\, \Gamma_0 \quad (\text{with } \ln \Gamma_0 = 1.22)$$

or

$$k_B T_c = 0.57 \times \Delta(^1S_0).$$

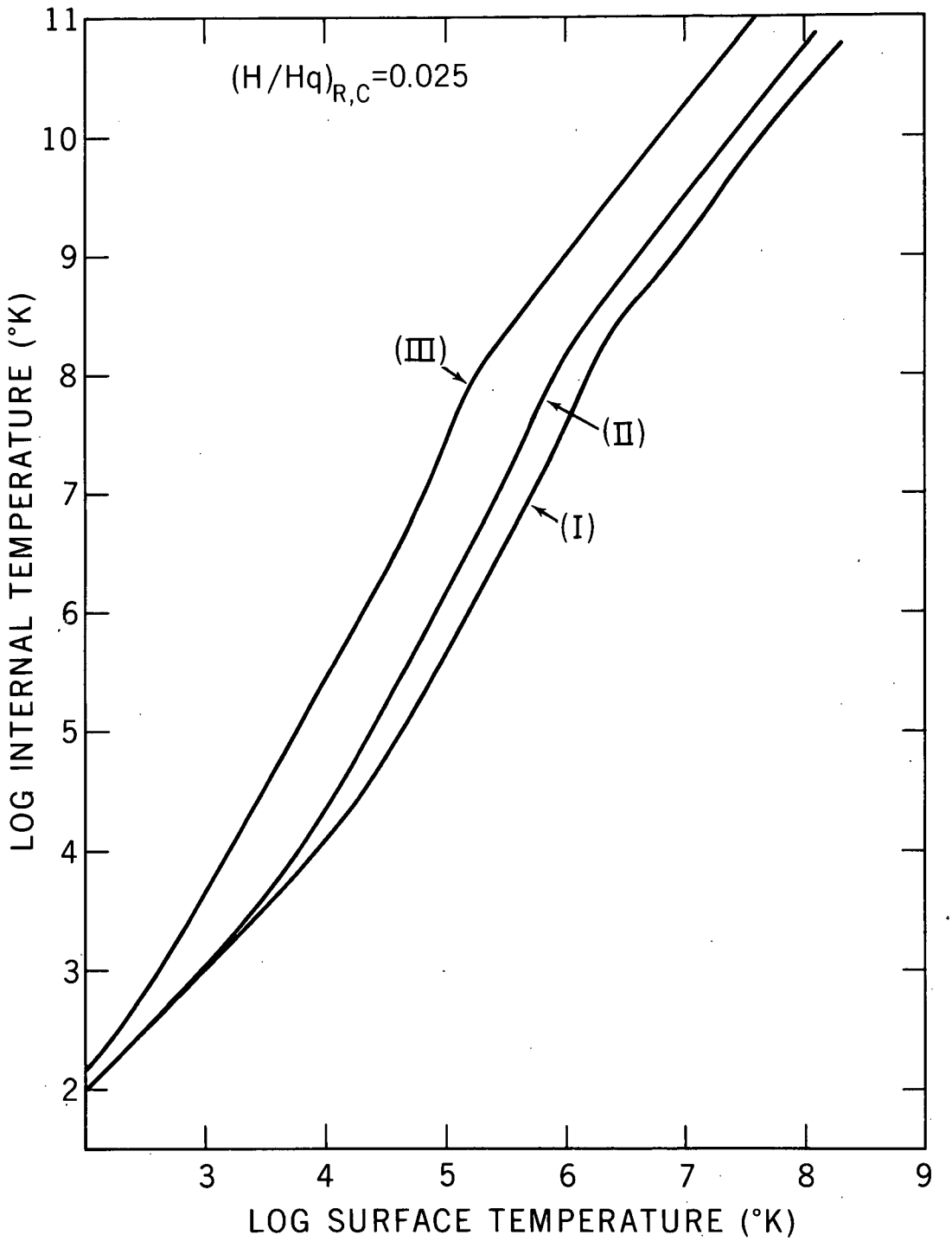

Figure 6. Internal temperature as a function of surface temperature for the three dense star models (I), (II), and (III) chosen in section III(b). A uniform magnetic field of strength $(H/H_q) = 0.025$ is used.

Y_s is a superfluid correction factor which becomes unity in the absence of superfluidity. The intermediate region between $T = T_c$ and $T << T_c$ was interpolated. Thermal energy of heavy ions is expressed as

$$U^N_{ion} = \left[\int c_v \, n_{ion} \, 4\pi r^2 \, dr\right] T, \quad \text{where}$$

$$c_v = a_i k_B \mathbb{D}\left(\frac{\theta}{T}\right), \tag{10}$$

$$a_i = \frac{3}{2} \quad \text{for} \quad T \geq T_g \quad \text{and}$$

$$a_i = 3 \quad \text{for} \quad T \leq T_m.$$

T_g is the temperature above which ions become a gas and T_m is melting temperature. In the intermediate region between T_g and T_m, they become liquid and the constant a_i also takes the intermediate values between 1.5 and 3. The expression $\mathbb{D}(\theta/T)$ is the Debye function for crystals, which approaches zero as $(T/\theta)^3$ for $T << T_m$ (Landau and Lifshitz 1958). The values T_m and T_g were estimated from the work of Van Horn (1968) and Mestel and Ruderman (1967). In the above equations, k_B is Boltzmann's constant, and n_k and n_{ion} are number densities of particles k and ions, respectively. Other notation has the usual meaning.

The suppression of the URCA rates due to superfluidity was calculated by using the results of Itoh 1971, Itoh and Tsuneto 1972 , Wolf 1966 and Bahcall and Wolf 1965a. Itoh and Tsuneto (1972) also considered the URCA rates in subnuclear regions, and they were taken into account in our models. The recent work by Tsuruta, Truran and Cameron (1972) was used to take account of the URCA rates in the outermost layers (where $\rho < \rho_1$). These effects of heavy ions are generally negligible for heavier stars, but they become important for lighter stars.

The solid curve in Figure 7 shows the final, more realistic cooling curve for Model (II) which was obtained in the manner described above. To compare this result with the simplified version of the previous section, the dashed curves in Figure 7 show the two extreme cases, Case (S) (= exaggerated superfluidity) and Case (N) (= no superfluidity), for the same model.

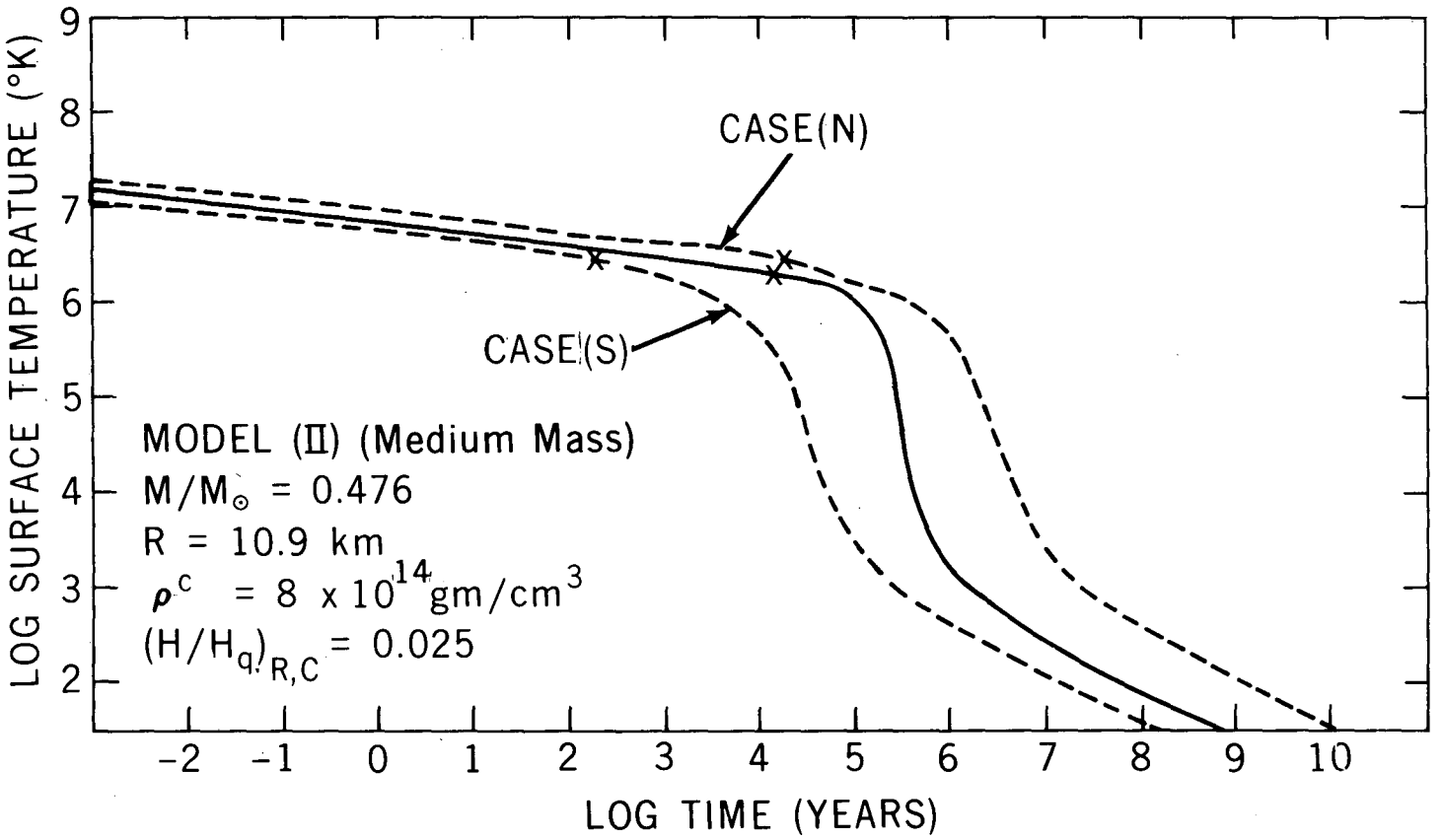

Figure 7. Cooling curves (surface temperature vs. time) for Model (II) of section III(b). The magnetic field strength is the same as in Figure 6. The dashed curves (S) and (N) are for maximum superfluidity and no superfluidity, respectively, as defined in section III(a). The solid curve is the final cooling curve obtained by the method described in section III(b). The crosses have the same meaning as in Figure 3.

Figure 8 shows the final cooling curves for our models (I), (II) and (III). We see that the lightest star (III) is cooler than others in earlier stages ($t \lesssim 10^5$ years) but the trend is reversed when the star becomes older. Model (II) is the coldest star in lower temperature regions where the effect of superfluidity becomes significant. At this point it may be pointed out that the major difference in cooling behavior comes from density difference rather than mass difference. For instance, Model (II) of the present section and the V_γ (II) model of the previous section, due to their approximately same densities, have similar cooling behavior even though the latter is more than twice as massive as the former. Among realistic dense star models developed by other authors, our models chosen here are closest to those constructed by Baym, Pethick and Sutherland (1971). (In the medium mass region our models are also similar to those constructed by Ikeuchi, et. al. (1971).)

Here we wish to emphasize the importance of heavy ions for lighter stars. The sudden drop of temperature takes place at the age of about 10^7 years for Model (III) in Figure 8 (where heavy ion energies are included). When U^N_{ion} is neglected in Equation (2), this sudden cooling occurs near 10^6 years (for the same model).

At the age of a few million years regarded as the average age of radio pulsars (e.g. Gunn and Ostriker 1970), the stars should be very cold. This conclusion is relatively independent of particular models used. This is because the transparency due to strong magnetic fields, which is the main cause for the sudden coolings, is achieved by this time. For those stars the surface temperatures are from several hundred to several thousand degrees (*2). Thus, the conclusion reached in our previous work (Tsuruta, et. al. 1972) is still valid. Thermal ionization of atoms in the atmosphere will be negligible and only residual rotational energy may be responsible for these older pulsars. This may then explain the lack of observed pulsars with periods longer than a few seconds (Ruderman 1971). These cold, dense stars seem to have a peculiar property, that we can see through the center from the two magnetic poles. It may be noted that the above conclusion was reached by temporarily disregarding Model (III). This is because neutron stars with mass less than about $0.2M_\odot$ may not be formed (Bethe 1972b, Cohen and Borner 1972). (This lightest model was chosen to dramatize the density dependence of cooling behavior.) The cooling behavior of a neutron star of about $0.2M_\odot$ is closer to our Model (II) than Model (III).

In Table II surface temperatures and internal temperatures of the three models are shown at a few interesting points during their cooling history. The first two points correspond to the approximate age of the Crab pulsar and Vela pulsar, respectively. There it seems likely that the star is hot enough so that thermal effect can be important. Earlier in this symposium it was reported that the pulsar glitch information allows some estimates of the mass of these

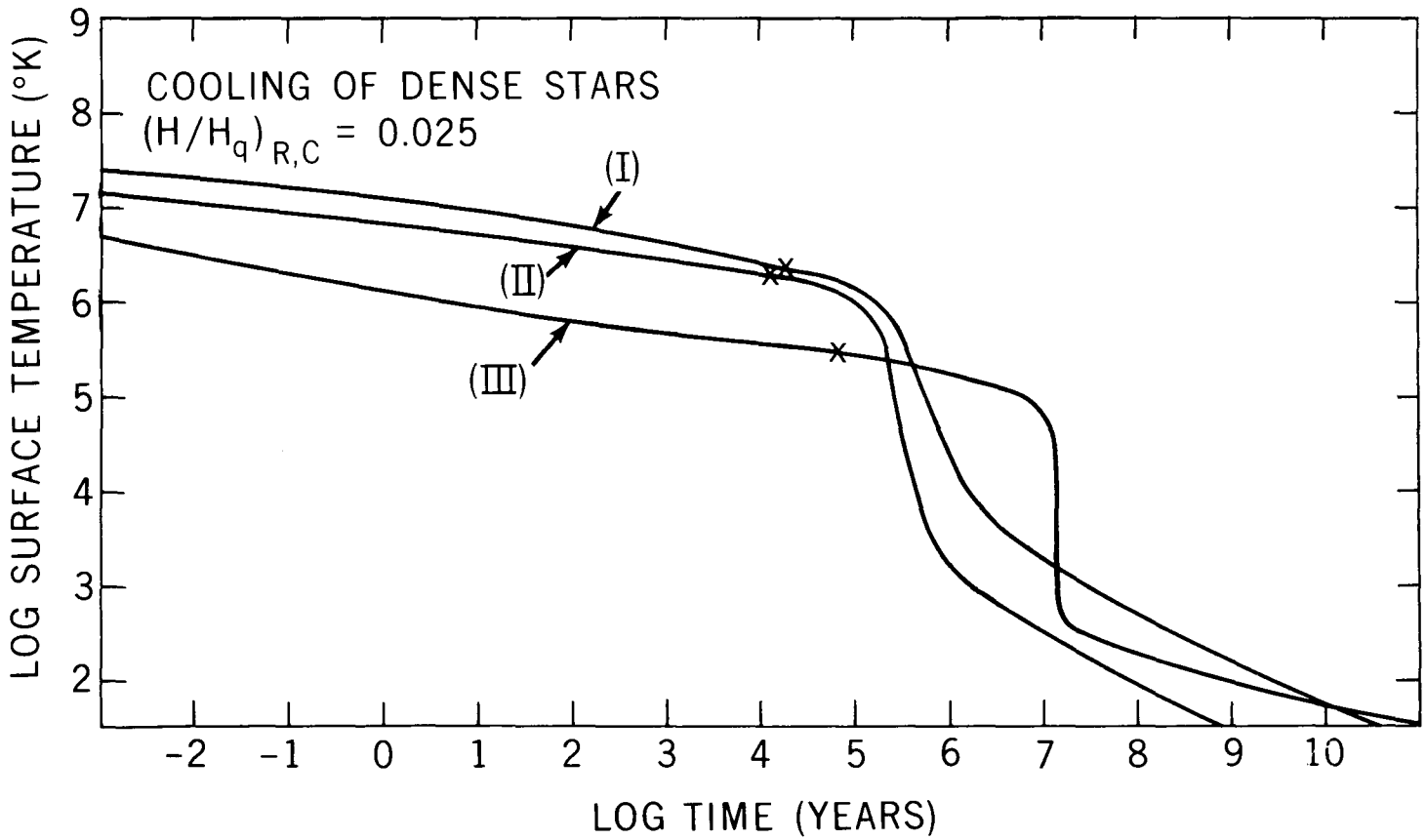

Figure 8. Final cooling curves (surface temperature vs. time) for the three models chosen in Section III(b), with the same magnetic field strength as in Figure 6. The crosses have the same meaning as in Figure 3.

TABLE II

Surface temperatures T_e and internal temperatures T_i for the models (I), (II) and (III) as described in Table I, at three interesting points during the cooling history.

	MODELS			AGE (years)	COMMENT
	(I)	(II)	(III)		
Log T_e (°K)	6.62	6.45	5.68	10^3	~CRAB
	6.40	6.30	5.56	10^4	~VELA
	4.38	3.21	5.21	10^6	
Log T_i (°K)	8.62	8.74	8.54	10^3	~CRAB
	8.36	8.54	8.38	10^4	~VELA
	4.58	3.26	7.92	10^6	

younger pulsars. The mass of the Crab pulsar estimated from the crustquake theory is about $0.5M_\odot$ (Pines 1972), while it is greater than $1M_\odot$ according to "accretion" theory (Borner and Cohen 1972). If the corequake theory applies, the Vela pulsar should be a heavy star (Shaham 1972). Therefore, we may expect to be able to detect X-rays from these pulsars. It is already known that the Crab Nebula has a X-ray pulsar, though its spectrum is not of blackbody radiation. As of now I am not aware of any conclusive report about the detection of pulsed X-rays from the Vela pulsar. However, caution may be advised for these young pulsars because nucleon superfluidity, on which above theories are based, may not yet be significant at their high temperatures. For instance, the Crab pulsar seems to be too hot for the effect of the $^3P_2$ superfluidity (see Table II). On the other hand, cooling will be much faster if pions are present (Bahcall and Wolf 1965b, Tsuruta 1972). It was already pointed out that pions may be present at high density regions (Bethe 1972a, Sawyer 1972, Scalapino 1972). Even though we do not know yet exactly at what density pions appear, it is possible that they are abundant for heavy hadron stars.

At this point we wish to consider the possible heating effect of crust-core rotation slippage. If a neutron star interiors are superfluid, frictional heat may be dissipated as its rotation is slowed. This process may keep the star hotter for longer periods. (Such a possibility was first suggested by Cameron (1970).) Greenstein (1971) estimated this effect and concluded that the effect can be significant enough so that thermal X-ray emission from certain pulsars may be detectable. The comparison shows that both for the Crab pulsar and Vela pulsar, the surface temperatures in his results and those obtained in this

section (Table II) are comparable if they are medium weight to heavy stars (the models (II) and (I). Greenstein suggests a few more older pulsars as other possible candidates for detection of X-rays due to this heating effect. Their surface temperatures estimated by Greenstein are in the vicinity of $(2 \sim 3) \times 10^5$ °K. At the ages which are expected for these pulsars, Model (III) is at comparable temperatures but our models (II) and (I) are colder (with their surface temperatures at $10^3 \sim 2 \times 10^5$ °K). (We may comment that the magnitude of the frictional effects depends on the strength of the coupling between the charged and the superfluid components of the stars and that its quantitative estimates are not yet available.)

(c) Cooling of White Dwarfs

Before closing we wish to show typical cooling curves of white dwarfs. The properties of the particular model chosen here are listed in Table III. This is the same model as the one chosen in Tsuruta and Cameron 1970, and further details are found in that paper. A rather massive white dwarf star was chosen so that it can possess a URCA shell. However, other neutrino processes (Beaudet, Petrosian and Salpeter 1967, Hansen 1968) are also included here. The cooling curves thus obtained are shown in Figure 9. A simple ideal gas was assumed for the straight line, while the other curve includes the effect of crystallization.

TABLE III

Properties of the White Dwarf Model Chosen in Section III(c)

Mass = 1.373 $M_\odot$ Central density = $10^{9.5}$ gm/cm^3 Radius = 1810 km Radius of URCA shell = 377 km URCA nuclear pair Na^{23} and Ne^{23} Core of 1$M_\odot$ of carbon-burning products Envelope of C^{12}		
Composition of Core		
Mass number	Mass fraction	Nuclei and electron capture thresholds (MeV)
16	0.01	O^{16} (10.4) C^{16}
20	0.41	Ne^{20} (7.03) O^{20} (21.22) C^{20}
23	0.06	Na^{23} (4.4) Ne^{23} (11.15) F^{23} (13.87) O^{23}
24	0.52	Mg^{24} (5.52) Ne^{24} (15.91) O^{24}

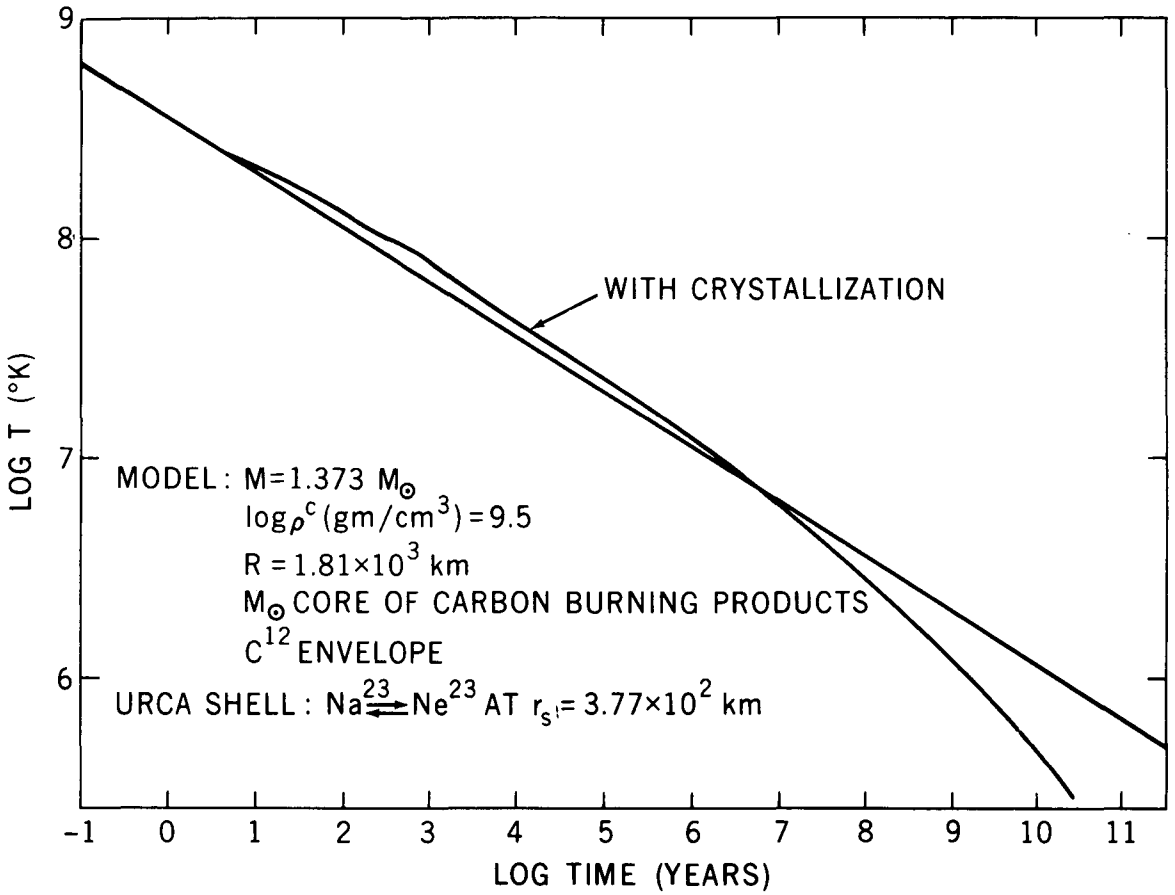

Figure 9. Cooling curves (internal temperature vs. time) for the white dwarf model chosen in section III(c).

I wish to thank the many persons mentioned in this paper and other participants of this symposium for valuable suggestions and discussions. The last part of this paper was completed during my visit at Aspen Center for Physics.

REFERENCES

Bahcall, J. N., and Wolf, R. A. 1965a, Phys. Rev., 140, B1452.

Bahcall, J. N., and Wolf, R. A. 1965b, Phys. Rev. Letters, 14, 343.

Baym, G., Bethe, H. A., and Pethick, C. J. 1971, Nucl. Phys., A175, 225.

Baym, G., Pethick, C. J., and Sutherland, P. 1971, Ap. J., 170, 299.

Beaudet, G., Petrosian, V., and Salpeter, E. E. 1967, Ap. J., 150, 979.

Bethe, H. A. 1972a, Proceedings of IAU Symposium No. 53, Physics of Dense Matter, to be published.

Bethe, H. A. 1972b, private communication.

Borner, G., and Cohen, J. M. 1972, to be published.

Cameron, A. G. W. 1970, private communication.

Canuto, V. 1970, Ap. J., 160, L153.

Canuto, V., and Chiu, H.-Y. 1969, Phys. Rev., 188, 2446.

Canuto, V., Lodenquai, J., and Ruderman, M. 1971, Phys. Rev., D3, 2303.

Cohen, J. M., and Borner, G. 1972, to be published.

Ginzburg, V. L. 1971, Physica, 55, 207.

Gold, T. 1968, Nature, 218, 731.

Greenstein, G. 1971, Nature Phys. Sci., 232, 117.

Gunn, J. E., and Ostriker, J. P. 1970, Ap. J., 160, 979.

Hansen, C. J. 1968, Astrophys. Spa. Sci., 1, 499.

Hartle, J. B., and Thorne, K. S. 1968, Ap. J., 153, 807.

Hayashi, C. 1971, private communication.

Ikeuchi, S., Nagata, S., Mizutani, T., and Nakazawa, K. 1971, Progr. Theor. Phys., 46, 95.

Itoh, N. 1971, private communication.

Itoh, N., and Tsuneto, T. 1972, Progr. Theor. Phys., 48, No. 6a, to be published.

Landau, L. D., and Lifshitz, E. M. 1958, Statistical Physics (Addison-Wesley Pub. Co., Mass.).

Lodenquai, J., Ruderman, M., Canuto, V., and Tsuruta, S. 1972, to be published.

Mestel, L., and Ruderman, M. 1967, Mon. Not. RAS, 136, 27.

Moszkowski, S. A. 1972, paper presented at APS Meeting, April, Wash. D. C. (Bulletin of APS, 17, 502).

Pandharipande, V. R. 1971, Nucl. Phys., A178, 123.

Pines, D. 1972, Proceedings of IAU Symposium No. 53, Physics of Dense Matter, to be published.

Ravenhall, D. G., Bennett, C. D., and Pethick, C. J. 1972, "Nuclear Surface Energy and Neutron Star Matter," preprint.

Ruderman, M. 1971, Phys. Rev. Letters, 27, 1306.

Ruderman, M., 1972, Proceedings of IAU Symposium No. 53, Physics of Dense Matter, to be published.

Salpeter, E. E. 1961, Ap. J., 134, 669.

Sawyer, R. F. 1972, Phys. Rev. Letters, 29, 382.

Scalapino, D. J. 1972, Phys. Rev. Letters, 29, 386.

Schatzman, E. 1958, White Dwarfs (North-Holland Pub. Co.).

Schwartzschild, M. 1958, Structure and Evolution of the Stars (Princeton U. Press).

Shaham, J. 1972, private communication.

Tamagaki, R. 1968, Progr. Theor. Phys., 39, 91.

Tamagaki, R. 1972, private communication.

Takatsuka, T. 1972, "Energy Gap in Neutron-Star Matter," preprint, NEAP-11, May, Kyoto University.

Tsuruta, S. 1964, Thesis, Columbia University.

Tsuruta, S. 1972, to be published.

Tsuruta, S., and Cameron, A. G. W. 1966a, Can. J. Phys., 44, 1863.

Tsuruta, S., and Cameron, A. G. W. 1966b, Can. J. Phys., 44, 1895.

Tsuruta, S., and Cameron, A. G. W. 1970, Astrophys. Spa. Sci., 7, 374.

Tsuruta, S., Canuto, V., Lodenquai, J., and Ruderman, M. 1972, Ap. J., 176, 739.

Tsuruta, S., Truran, J. W., and Cameron, A. G. W. 1972, to be published.

Van Horn, H. M. 1968, Ap. J., 151, 227.

Wheeler, J. A. 1966, Ann. Rev. Astron. and Astrophys., 4, 393.

Wolf, R. A. 1966, Ap. J., 145, 834.

NOTES

(*1) This is for a certain baryon-baryon interaction which he calls the "Modified Delta Interaction". However, for a Reid soft core baryon-baryon interaction with a G-matrix calculated by Sawada and Wong (private communication), there appear significant fractions of hyperons at supernuclear densities (Moszkowski, private communication). (However, both interactions lead to very similar equations of state for pure neutron matter.)

(*2) However, surface may be kept at somewhat above 10^5 °K if we take into account the heating by accretion of interstellar matter (Ramaty, private communication).

* U.S. GOVERNMENT PRINTING OFFICE: 1972—736-963/24T